Sustainable Structures
ISSN: 2789-3111 (Print); ISSN: 2789-312X (Online)
http://www.sustain-dpl.com/journal/sust
DOI: 10.54113/j.sust.2026.000105

ORIGINAL ARTICLE

Study on properties of one-part fly ash/slag based geopolymer mortars modified by cellulose nanocrystals

Aofei Guo[a], Haowei Ma[a], Wenming Yang[b], Hu Feng[a], Liusheng Chu[a,*], Zhihui Sun[c], Zhenyun Yu[a]

[a]School of Civil Engineering, Zhengzhou University, Zhengzhou, 450001, China
[b] School of Civil Engineering, Tianjin University, Tianjin, 300072, China
[c] Civil and Environmental Engineering Department, University of Louisville, Louisville, KY 40292, USA
[*]Corresponding Author: Liusheng Chu. Email: chuliusheng@zzu.edu.cn

Abstract: In this study, a small amount of cellulose nanocrystals (CNC) were added to fly ash (FA)/granulated ground blast furnace slag (GGBS)-based geopolymer mortars to investigate the performance influence and action mechanism of the modified FA/GGBS-based geopolymer mortar by CNC. The results showed that following a 28-day curing, the best mechanical performance was achieved when the FA/GGBS mass ratio was 3:7; compared to the 5:5 mass ratio of FA/GGBS, the compressive strength and flexural strength increased by 14.96% and 40.74%, respectively; and compared to the 7:3 mass ratio of FA/GGBS, the compressive strength and flexural strength increased by 112.12% and 80.95%, respectively. However, with higher GGBS proportions, the flowability decreased. Additionally, the effect of CNC was inconsistent in systems. At 3-day curing age, in the FA/GGBS=3:7 and 5:5 systems, the addition of CNC inhibited the strength development of geopolymer mortars, whereas in the FA/GGBS=7:3 system, it slightly accelerated the strength development. However, after 28 days of curing, the strength of the geopolymer mortars under all conditions increased to varying degrees after the addition of CNC. Microstructural tests via scanning electron microscopy-energy dispersive spectroscopy (SEM-EDS) and isothermal calorimetry (IC) showed that increasing GGBS content and adding CNC enhanced the reaction activity and structural compactness of FA/GGBS-based geopolymer mortars.

Keywords: geopolymer, fly ash, granulated ground blast furnace slag, cellulose nanocrystal

1 Introduction

As the construction material of choice worldwide, concrete holds unparalleled dominance, and Portland cement (OPC), a key raw material in concrete production, has become an indispensable industrial product in our daily lives. However, during OPC production, limestone calcination generates substantial CO_2 emissions. According to research by Peng et al. [1], producing 1 kg of OPC results in 0.66–0.82 kg of CO_2 emissions, with OPC production contributing 5–7% of global carbon emissions. As global climate change intensifies and awareness of green and sustainable development grows, there is an urgent need to find a green, low-carbon cementitious material to replace OPC.

Geopolymers, widely discussed in recent years, hold great potential as substitutes for OPC. The term “geopolymer” was originally proposed by Davidovits [2] to describe a class of inorganic polymer

Received: 13 June 2025; Received in revised form: 6 August 2025; Accepted: 8 May 2026

materials with a three-dimensional mesh-like structure, similar to zeolites. The main sources of the materials for geopolymer are natural minerals containing silicate-aluminate or industrial waste materials (such as fly ash, slag and steel slag, etc.). Under ambient or slightly elevated temperatures, these materials react with alkali activators to form a three-dimensional mesh-like cementitious material composed of alternating $[SiO_4]^{4-}$ and $[AlO_4]^{5-}$ tetrahedral units linked by shared oxygen atoms [3, 4]. Unlike OPC, geopolymer production does not require the calcination of limestone. Using geopolymer materials instead of OPC as the cementitious material can reduce greenhouse gas emissions by 73% and energy consumption by 43% [5].

Existing studies have demonstrated that fly ash-based geopolymers are a viable alternative to OPC. However, further research is still required to enhance their commercial viability and reliability. A common approach involves incorporating additives into FA-based geopolymers to improve their structure and performance. Examples include cellulose nanocrystals (CNCs), nano-silica, and carbon nanotubes (CNTs). However, only CNCs are bio-based, offering low environmental impact and align ing with the principles of green and sustainable development. Thus, this investigation employs CNCs as additives to explore their modification mechanisms in FA-based geopolymers. CNCs are derived from plants such as cotton, wood, and flax [6] and offer advantages such as excellent physical and chemical properties, environmental friendliness, low cost, and high elastic modulus [7, 8]. Studies indicate that CNCs not only possess nucleation and bridging effects typical of one-dimensional nanomaterials but also exhibit unique effects such as short-circuit diffusion and spatial hindrance, promoting the formation of highly ordered and dense C-S-H gels, thereby enhancing the performance of cementitious materials [9-13]. Moreover, according to Rahmawati [14], adding CNCs to high-calcium fly ash-based geopolymers improves their mechanical properties. Specifically, a 0.1% addition of CNCs increased compressive and tensile strengths by 15.76% and 11.72%, respectively. And Feng et al. found that incorporating 0.3% CNC into alkali-activated fly ash/slag pastes enhanced the compressive strength by 18.54% (8% alkaline activator) and 16.99% (4% alkaline activator), while the flexural strengths by 60.87% (8% alkaline activator) and 50.12% (4% alkaline activator) after 28 days of curing [15].

However, for geopolymer materials to achieve widespread application, both excellent mechanical properties and simplified preparation processes are required. Traditional two-part geopolymers consist of pre-prepared alkali activator solutions and solid aluminosilicate precursors. The preparation involves safely handling corrosive alkali solutions and then mixing them with the precursor, making the process complex and less practical for large-scale applications [16]. To address this, researchers have developed one-part geopolymers that require only water addition, making their usage similar to OPC [17]. One-part geopolymers are prepared by mixing solid alkali activator powders with solid aluminosilicate precursors, and then simply adding water to the mixture [16].

In this study, FA and GGBS were used as mineral admixtures, fast-dissolving granular anhydrous sodium metasilicate powder was employed as the alkali activator material in combination with standard quartz sand to prepare one-part geopolymer mortar. The FA/GGBS mass ratio (3:7, 5:5, and 7:3) and CNC content (0%, 0.05%, 0.10%, 0.20%, and 0.30% by mass of mineral admixtures) were used as variables to study their effects on the mechanical and workability properties of one-part FA/GGBS-based geopolymer mortar. Finally, the mechanisms were further analyzed through isothermal calorimetry and scanning electron microscopy experiments.

2 Materials and experiments

2.1 Materials

2.1.1 Mineral admixtures

The mineral admixtures used in this research include Class I fly ash (FA) provided by Henan Dengfeng Huarun Power Co., Ltd. and S95 granulated blast furnace slag (GGBS) supplied by Changwang Mineral Products Co., Ltd., Lingshou County, Hebei Province. **Fig. 1** Presents SEM micrographs of mineral admixtures. From the SEM images, it can be observed that Fly ash exhibits a

characteristic spherical particle morphology, while GGBS exhibits irregular shapes. **Tab. 1** details the chemical compositions of mineral admixtures.

Table 1. Chemical composition of mineral admixtures (%)

Materials	SiO_2	$Al2O_3$	CaO	MgO	SO_3	TiO_2	Fe_2O_3	Na_2O	K_2O	P_2O_5
FA	52.949	31.479	4.493	0.766	1.608	1.370	4.102	0.458	2.188	0.359
GGBS	30.217	15.684	40.937	8.067	2.096	1.452	0.371	0.443	0.380	0.013

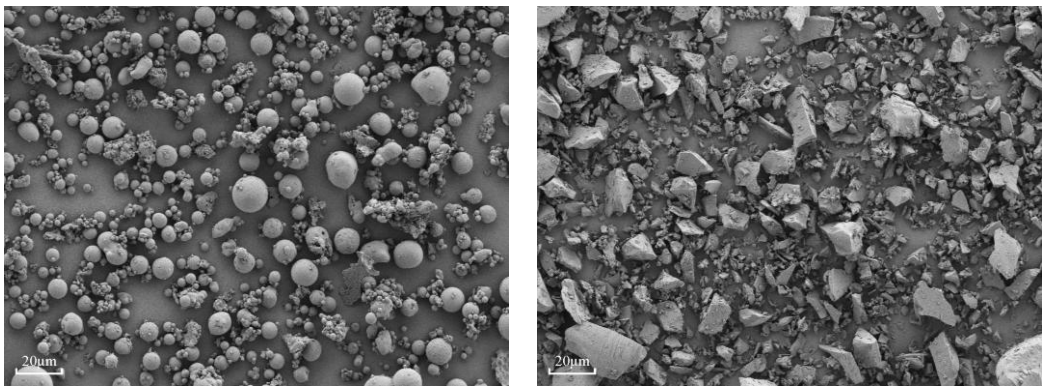

(a) FA (b) GGBS

Fig. 1. SEM of mineral admixtures

The FA and GGBS were analyzed using X-ray diffraction (XRD), as shown in **Fig. 2(a)**. The XRD patterns indicate that the crystalline substances in FA primarily include quartz, mullite, hematite, and calcium oxide, whereas GGBS predominantly contains an amorphous glassy phase. The crystallinity of FA and GGBS are 62.36% and 45.57%, respectively. The gradation curves of FA and GGBS are displayed in **Fig. 2(b)**. The average particle size (D_{AV}) and median particle size (D_{50}) of FA are 22.47 μm and 9.75 μm, respectively, with a specific surface area of 1.88 m^2/g; for GGBS, the average particle size (D_{AV}) and median particle size (D_{50}) are 13.05 μm and 9.75 μm, respectively, with a specific surface area of 2.06 m^2/g.

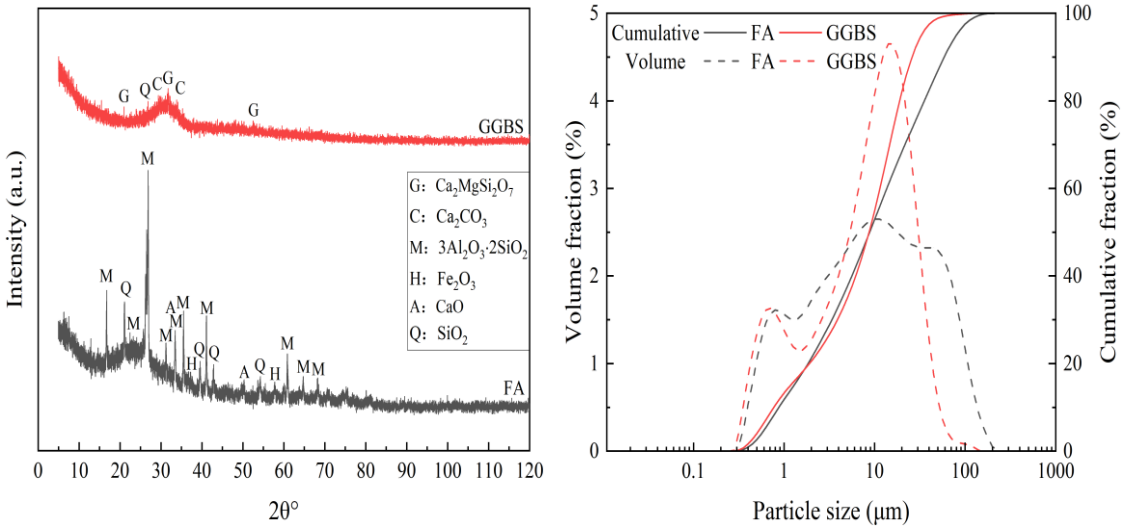

(a) XRD pattern (b) Particle size distribution

Fig. 2. XRD pattern and particle size distribution of FA and GGBS

2.1.2 Fine aggregate

The fine aggregate used in the study is Chinese ISO standard sand produced by Xiamen ISO Standard Sand Co., Ltd., with a SiO_2 content greater than 98%, a moisture content below 0.18%, a mud content below 0.18%, a loss on ignition below 0.47%, a chloride ion content below 0.0070%, and a

floating matter content below 0.0020%. The particle size distribution curve of the sand is shown in **Fig. 3**.

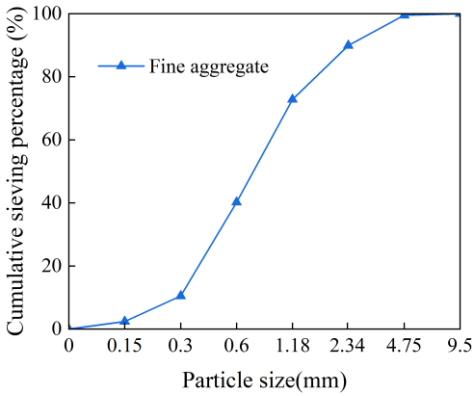

Fig. 3. Particle size distribution of fine aggregates

2.1.3 Alkali-activator

The alkali activator used in this study is fast-dissolving granular anhydrous sodium metasilicate produced by Qingdao Gulf Chemical Co., Ltd. The composition and content of the activator are provided in **Tab. 2**.

Table 2. Composition and content of anhydrous sodium metasilicate

Material	Modulus	Na_2O (%)	SiO_2 (%)	Baumé (%)	Density (g/cm^3)	Water insoluble (%)	Iron content (ppm)
anhydrous sodium metasilicate	1.0	50.88	46.45	95.82	1.10	0.011	68

2.1.4 Cellulose nanocrystals

The cellulose nanocrystals (CNCs) used in this study are supplied by CelluForce Inc., Canada. The CNC material has a moisture content of 3.7%. **Fig. 4** displays the XRD pattern and morphology of raw CNC materials, and the crystallinity index of the CNC material, calculated using this pattern and Eq. (1), is determined to be 70.80%. The diameter and length of CNC are around 5 nm and 100 nm respectively. The aqueous solution of the CNC material has a pH of 6.8 and a conductivity of 238 $\mu S \cdot cm^{-1}$.

$$I_c = \frac{I_{002} - I_{am}}{I_{002}} \times 100\% \quad (1)$$

where I_{002} is the peak intensity at a 2θ value around 22°, representing the crystalline component; I_{am} is the valley intensity at a 2θ value around 18°, representing the amorphous component; I_c is the crystallinity index.

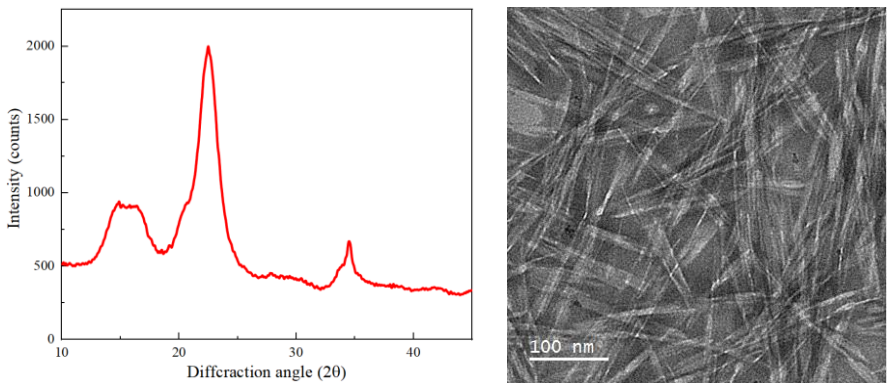

(a) (b)

Fig. 4. (a) XRD spectrum and (b) morphology of CNC

2.2 Mixture proportions

This paper studies the mechanical and workability properties of CNC-modified FA/GGBS-based geopolymer mortar. Focus on the influence of the FA/GGBS mass ratio and the CNC content on the performance of FA/GGBS-based geopolymer mortars. Based on preliminary experiments, three FA/GGBS mass ratios (3:7, 5:5, and 7:3) were selected according to differences in the initial setting time of the slurry under varying FA/GGBS ratios. The CNC dosages were determined based on the findings of Roopchund [18, 19], which indicated that CNC concentrations below 0.5% enhance the development of mechanical properties in geopolymers. Thus, the water-to-binder ratio (*w*/*b*) is set to 0.5. The modulus of the alkali activator is set at 1.0 and an alkali equivalent (calculated as Na_2O content) of 6% is used. The experimental variables are the FA/GGBS mass ratio (3:7, 5:5, and 7:3) and CNC content (0%, 0.05%, 0.10%, 0.20%, and 0.30%, by mass of the mineral admixtures). The specimens are named as "FaGbCc," where "a" and "b" represent the ratio of FA and GGBS in the mineral admixtures (with the total mass of mineral admixtures normalized to 10), and "c" denotes the CNC content. The mixture proportions are provided in **Tab. 3**.

Table 3. Mixture proportions of cellulose nanocrystal modified geopolymer mortars

Mix	Water	FA	GGBS	Fine aggregate	Alkali-activator (Na_2O content)	CNC (%)
F3G7C0	5	3	7	30	0.6	0
F3G7C0.1						0.1
F3G7C0.2						0.2
F3G7C0.3						0.3
F5G5C0	5	5	5	30	0.6	0
F5G5C0.1						0.1
F5G5C0.2						0.2
F5G5C0.3						0.3
F7G3C0	5	7	3	30	0.6	0
F7G3C0.1						0.1
F7G3C0.2						0.2
F7G3C0.3						0.3

2.3 Sample preparation

For solutions requiring CNC addition, the pre-weighed CNC is mixed with the required amount of water and stirred using an electric mixer at 400 rpm for 5 minutes. The mixture is then ultrasonically dispersed for 10 minutes using an ultrasonic disperser (produced by Ningbo Xin zhi Biotechnology Co., Ltd.) to obtain the desired solution.

For the preparation of mortar specimens, the pre-weighed FA, GGBS, and granular anhydrous sodium metasilicate are poured into a planetary cement mortar mixer (Model: JJ-55, manufactured by Wuxi Huaxi Construction Material Testing Equipment Co., Ltd.) and dry-mixed for 30 seconds to ensure thorough mixing. Next, the pre-weighed water or prepared CNC solution is added, followed by low-speed mixing for 0.5 minutes. Within the next 0.5 minutes, the pre-weighed ISO standard sand is gradually added while mixing at low speed. The mixture is then mixed at low speed for 1 minute and subsequently at high speed for another 1 minute to ensure uniform and thorough mixing.

The mixed slurry is poured into the required molds, which are placed on a vibration table for compaction to achieve a dense structure in two stages. After the specimens are molded and surface-finished, they are immediately covered with plastic film and allowed to rest in an indoor environment at 20℃ ± 5℃ and relative humidity >50% for 24 hours. After demolding, the specimens are transferred to a curing chamber maintained at 20℃ ± 2℃ and relative humidity >95% until the specified curing age is reached. Subsequent tests, such as mechanical performance evaluation, are conducted thereafter.

2.4 Experiments

2.4.1 Flowability test

The geopolymer mortar's flow properties were assessed using GB/T 1346-2011 [20]. After the

FA/GGBS- based geopolymer slurry has been mixed as per Section 2.3, the flow table test should be conducted immediately. The testing apparatus was a cement mortar flowability tester (Model: NLD-3). The timing for this test began when water was added to the geopolymer mortar, and the entire procedure was completed within 6 minutes.

2.4.2 Mechanical tests

(1) Flexural strength test

The geopolymer mortar's flexural strength were assessed using GB/T 17671-2021 [21]. The test used prismatic specimens with dimensions of 40 × 40 × 160 mm³, with three specimens in each group. The flexural strength of samples with different FA/GGBS ratios and CNC contents was measured.

(2) Compressive strength test

The geopolymer mortar's compressive strength were assessed using GB/T 17671-2021 [21]. After the flexural strength test, two halves of each broken specimen were used for the compressive strength test.

2.4.3 Isothermal calorimetry (IC) test

The reaction heat of geopolymer samples with different FA/GGBS ratios and CNC contents was tested using an isothermal calorimeter (Model: TAM Air, manufactured by TA Instruments, Waters Technology (Shanghai) Co., Ltd.). The test was conducted under constant temperature conditions (25 ± 0.1°C) for 72 hours. The instrument was connected to a computer for data acquisition. The heat release and heat release rate curves were recorded to investigate the exothermic reaction process of the FA/GGBS-based geopolymer.

2.4.4 Scanning electron microscopy-energy dispersive spectroscopy (SEM-EDS) test

The microstructure and composition of geopolymers with different FA/GGBS ratios and CNC contents were characterized using SEM-EDS. The sample preparation involved the following steps: (1) soaking the sample in isopropanol for 24 hours; (2) replacing the isopropanol and soaking for an additional 3 days to displace free water in the sample; (3) drying the sample in a vacuum oven at 60°C until constant weight was achieved; (4) storing the sample in a vacuum environment to avoid carbonation before testing.

3 Results and discussions

3.1 Flowability test

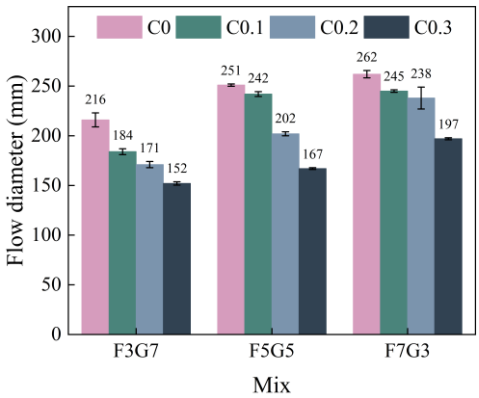

Fig. 5. Flow diameter of CNC-modified FA/GGBS-based geopolymer mortars

The flowability results of CNC-modified FA/GGBS-based geopolymer mortars are shown in **Fig. 5**. As the FA content increases, the flowability improves significantly. The flow diameter of F3G7C0 and F7G3C0 are 216 mm and 262 mm, respectively, with an increase of 21.3%. This is because GGBS contains higher levels of CaO, which leads to higher reactivity compared to FA, causing the slurry to

set and harden more rapidly. Additionally, as can be seen from **Fig. 1** in Section 2.1, GGBS powder particles have sharp edges and are extremely irregular, compared to the smooth spherical structure of FA, the morphology of GGBS is less conducive to the flow of the polymer slurry. This observation aligns with findings from other studies [22].

Increasing the CNC content reduces the flowability of the geopolymer mortars. For F3G7, F5G5, and F7G3, the flow diameter reduces from 216 to 152 mm, from 251 to 167 mm, and from 262 to 197 mm, respectively. This reduction in flowability is attributed to three factors: (1) the elongated shape of CNC introduces interparticle resistance, lowering the flowability of the geopolymer; (2) as the CNC concentration increases, agglomeration within the system further reduces the flowability of the geopolymer mortar [11]; (3) the hydrophilic property of CNC enables it to absorb some water, reducing the content of free water available.

3.2 Mechanical properties

3.2.1 Compressive strength

Fig. 6 plots compressive strength development of CNC-modified FA/GGBS-based geopolymer mortars at different curing ages. From **Fig. 6**, it can be evidenced that the compressive strength of geopolymer mortars increases with the increase in the content of GGBS, regardless of the curing age, whether at 3 days (**Fig. 6(a)**) or 28 days (**Fig. 6(b)**). As shown in **Fig. 6(a)**, following a 3-day curing, the compressive strength of F3G7C0 and F5G5C0 increases by 293.20% and 184.47%, respectively, compared to F7G3C0. According to **Fig. 6(b)**, following a 28 days curing, the compressive strength of F3G7C0 and F5G5C0 increases by 112.12% and 84.51%, respectively, compared to F7G3C0. This result was also obtained in the study by Feng et al. [23]. This is because in the FA/GGBS-based geopolymer slurry, the CaO mainly comes from GGBS. The content of CaO in the system increases with the increase of GGBS content, leading to the formation of more C-S-H and C-A-S-H gels in the system, This provides additional nucleation sites for the formation of the geopolymer, allowing the silicon and aluminum components in the system to dissolve and precipitate more effectively, thereby accelerating the geopolymerization process [24-26].

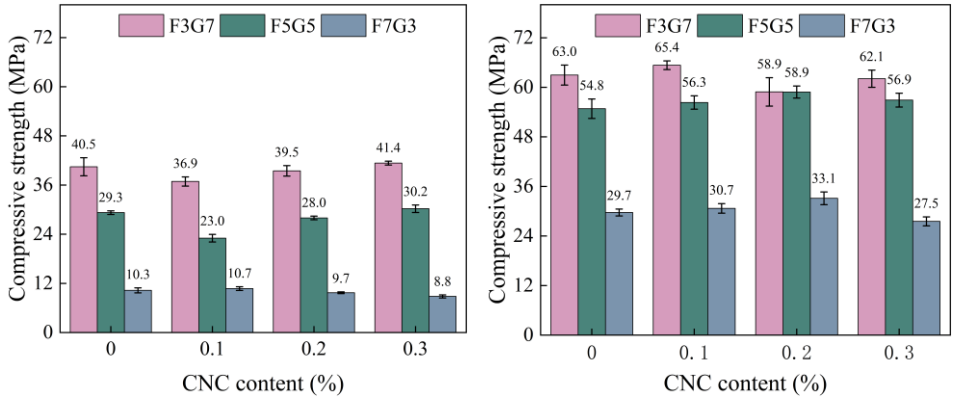

(a) Curing for 3-day (b) Curing for 28-day

Fig. 6. Compressive strength of CNC-modified FA/GGBS-based geopolymer mortars

From **Fig. 6(a)**, it can be seen that in the early stage (3-day curing), compared to specimens without CNC, CNC primarily exerted an inhibitory effect on the compressive strength of the samples. However, as the content of CNC was increased from 0.1% to 0.3%, the compressive strength of F3G7 and F5G5 gradually increased, while the compressive strength of F7G3 showed little change. Taking the F5G5 sample as an example, compared to F5G5C0, the compressive strength of F5G5C0.1 and F5G5C0.2 decreased by 21.34% and 4.41%, respectively, while the compressive strength of F5G5C0.3 showed negligible change. However, as shown in **Fig. 6(b)**, following a 28-day curing, CNC exhibited a slight enhancement on the compressive strength of FA/GGBS-based geopolymer mortars. Taking the F5G5 sample as an example, compared to F5G5C0, the compressive strength of F5G5C0.1, F5G5C0.2, and F5G5C0.3 increased by 2.74%, 7.35%, and 3.79%, respectively. This might be because it was during the later stage of the reaction, when water becomes insufficient, CNC begins to play a role in short-circuit diffusion [9, 11, 13], accelerating the dissolution rate of fly ash and slag particles and the release

of ions such as Ca^{2+}, Al^{3+}, and Si^{4+}, which enhances the compressive strength of the sample.

3.2.2 Flexural strength

Fig. 7 plots flexural strength development of CNC-modified FA/GGBS-based geopolymer mortars at different curing ages. Consistent with compressive trends, As can be seen from **Fig. 7**, with the increase of GGBS content in the system, the flexural strength of FA/GGBS-based geopolymer mortars has improved to varying degrees. For instance, after 28-day curing, the flexural strength of F7G3C0 is 4.15 MPa, while the flexural strengths of F5G5C0 and F3G7C0 are 5.43 MPa and 7.60 MPa, representing increases of 30.84% and 83.13%, respectively.

As shown in **Fig. 7(a)**, when the CNC content changes, the early-stage flexural strength shows a similar trend to compressive strength, with CNC exerting an inhibitory effect on flexural strength. However, this inhibitory effect weakens as the CNC content increases. Under the F5G5 condition, when the CNC content is 0.00%, 0.10%, 0.20%, and 0.30%, the flexural strength of the geopolymer mortars specimens is 4.47 MPa, 3.60 MPa, 4.40 MPa, and 4.63 MPa, respectively. When the CNC content is 0.10%, the flexural strength decreases by 19.46%. In contrast, as shown in **Fig. 7(b)**, following a 28-day curing, the flexural strength of F5G5C0 and F5G5C0.1 is 5.40 MPa and 6.70 MPa, respectively. When the CNC content is 0.10%, the flexural strength of the F5G5 sample increases by 22.16%.

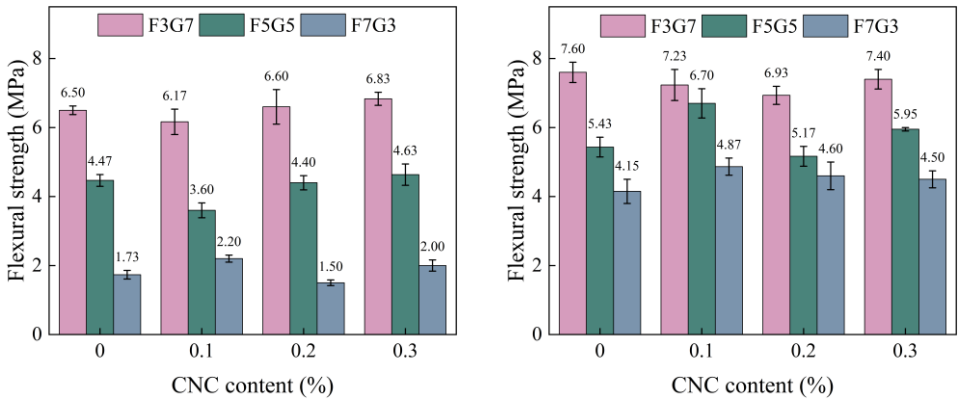

(a) Curing for 3-day (b) Curing for 28-day

Fig. 7. Flexural strength of CNC-modified FA/GGBS-based geopolymer mortars

3.3 Isothermal calorimetry

The geopolymerization process is a sophisticated process involving three steps: dissolution, precipitation, and polycondensation, which occur almost simultaneously [22]. However, based on the reaction heat rate curve of geopolymerization, the reaction process can be divided into the following five stages: (I) rapid reaction stage, (II) induction stage, (III) acceleration stage, (IV) deceleration stage, and (V) steady diffusion stage. The rapid reaction stage mainly involves the dissolution of precursors, while the acceleration stage primarily corresponds to the exothermic polymerization of dissolved monomers in the system [27]. The reaction heat curves of FA/GGBS-based geopolymers are shown in **Fig. 8**. Under varying FA/GGBS mass ratio and CNC content, the reaction heat rate curves exhibit a single exothermic peak, which mainly corresponds to the depolymerization and polycondensation of dissolved monomers in the system [28].

As shown in **Figs. 8(a)**, **8(b)**, and **8(c)**, the reaction exothermic rate and total exothermic amount of the FA/GGBS-based geopolymer slurry increase as the content of GGBS in the system increases. Without CNC addition, the peak heat release rates during the acceleration phase for the F7G3, F5G5, and F3G7 conditions are 0.414 mW/g, 1.050 mW/g, and 1.514 mW/g, respectively. When the GGBS content increases from 30% to 70%, The peak rate increased by approximately 2.5 times, indicating that during the acceleration phase, the F3G7 condition resulted in more dissolved monomers polymerizing into gel products. This aligns with the early-stage mechanical strength development rate observed in Section 3.2. **Figs. 6(a)** and **7(a)** in Section 3.2 show that after 3-day of curing, the flexural and compressive strengths of F3G7C0 far exceed those of the F7G3C0. In terms of total heat release, the values for F7G3C0, F5G5C0, and F3G7C0 are 143.73 J/g, 127.30 J/g, and 92.26 J/g, respectively. The total heat release of F3G7C0 increased by 55.79% compared to F7G3C0, further confirming the

superior mechanical performance of F3G7C0 over F7G3C0. According to the chemical compositions of mineral admixtures in Section 2.1.1, the CaO content in F3G7 is 30.01%, while that in F7G3 is only 15.43%. The high active CaO content in the F3G7 condition dissolves more monomers during the rapid reaction phase and promotes the polycondensation of additional gel materials during the acceleration phase. As shown in **Fig. 9** of Section 3.4, the SEM images of the F3G7 condition exhibit more flocculent and lamellar gel structures and fewer cracks compared to F7G3. The high active CaO content in GGBS accelerates the reaction rate and increases the heat release rate [29]. According to the geological polymer reaction heat release rate curve and total heat release curve shown in **Fig. 8**, combined with **Fig. 6** and **7** in Section 3.2, it can be observed that as the content of GGBS in the system increases, the address geopolymerization reaction of the paste becomes more rapid and complete, and the mechanical strength of the specimen also becomes higher.

The effect of CNC varies in systems with different FA/GGBS mass ratios. For FA/GGBS = 3:7 and 5:5, as shown in **Figs. 8(a)** and **8(b)**, adding CNC to the FA/GGBS based geopolymer slurry can increase the peak value of the reaction heat rate curve, but the total heat release does not show a significant improvement. In fact, for FA/GGBS = 5:5, the total heat release in systems with CNC is lower than in the system without CNC. Specifically, the peak heat release rates for F5G5C0, F5G5C0.1, F5G5C0.2, and F5G5C0.3 are 1.049 mW/g, 1.314 mW/g, 1.351 mW/g, and 1.372 mW/g, respectively, while their total heat release values are 59.747 J/g, 52.184 J/g, 53.586 J/g, and 53.087 J/g, respectively.

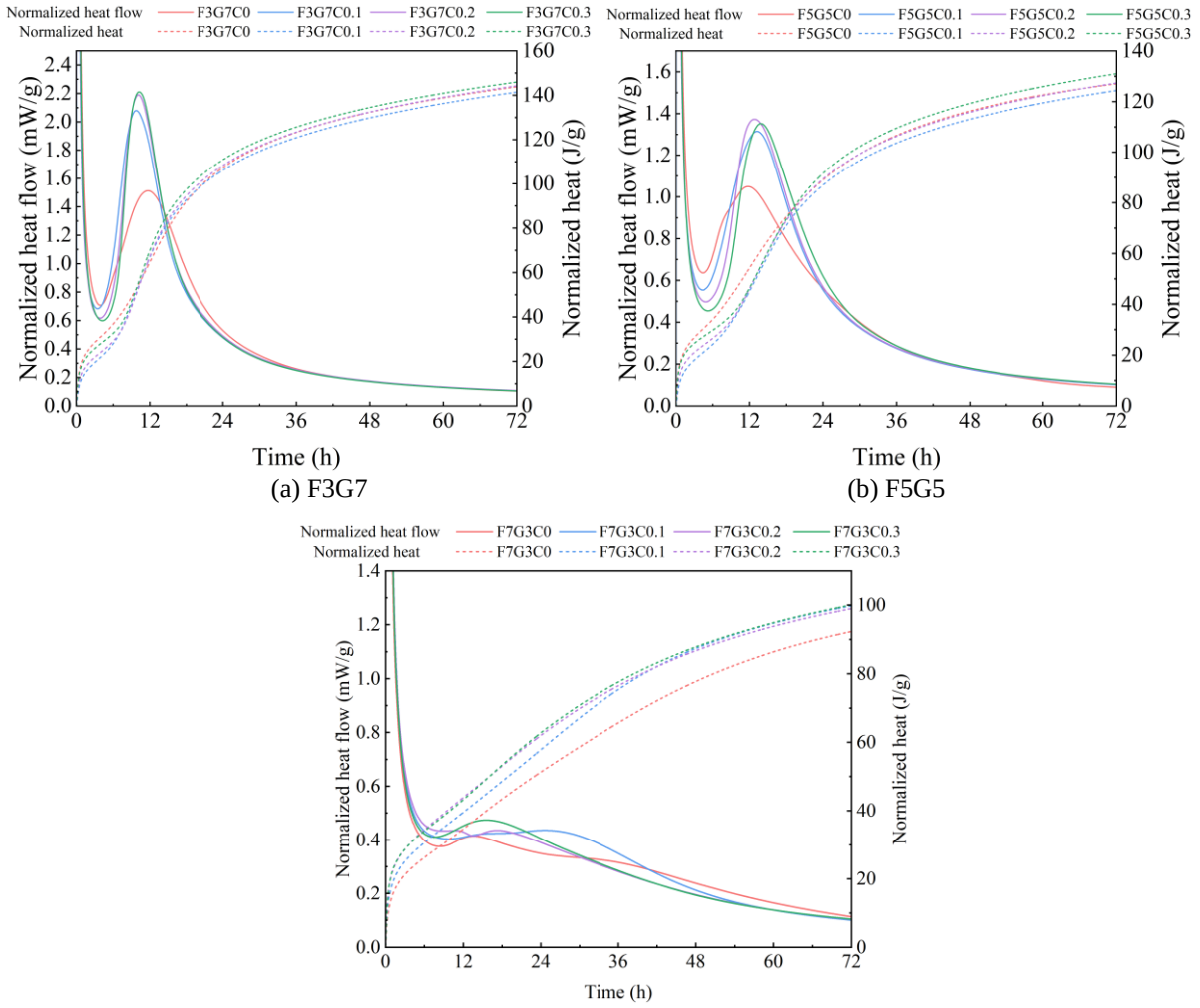

(a) F3G7 (b) F5G5

(c) F7G3

Fig. 8. Hydration heat release curve of CNC-modified FA/GGBS-based geopolymer

Fig. 8(c) shows that when FA/GGBS = 7:3, the addition of CNC not only increases the peak value of the exothermic curve but also raises the total heat release. This result was also obtained in the study by Feng et al. [15]. However, it differs from the results observed for FA/GGBS ratios of 3:7 and 5:5.

This discrepancy may be due to the higher FA content under the FA/GGBS = 7:3 condition. In this case, most of the CNC are adhered to the surface of the FA particles and has a limited impact on the dissolution rate of CaO. However, through a "short-circuit diffusion" effect, CNC promotes the total dissolution of Al_2O_3 and SiO_2 from FA, thereby increasing both the peak exothermic rate and the total heat release. This also explains why, at the early stages, only under the FA/GGBS = 7:3 condition does the addition of CNC enhance the mechanical performance of the system.

3.4 SEM-EDS analysis

To explore the influence laws of the FA/GGBS mass ratio and CNC content on the microstructure of FA/GGBS-based geopolymer mortars, and to correlate these findings with macroscopic mechanical properties, this study selected F3G7C0, F5G5C0, F7G3C0, and F5G5C0.1 for SEM-EDS analysis. **Figs. 9-12** present corresponding microstructural characteristics.

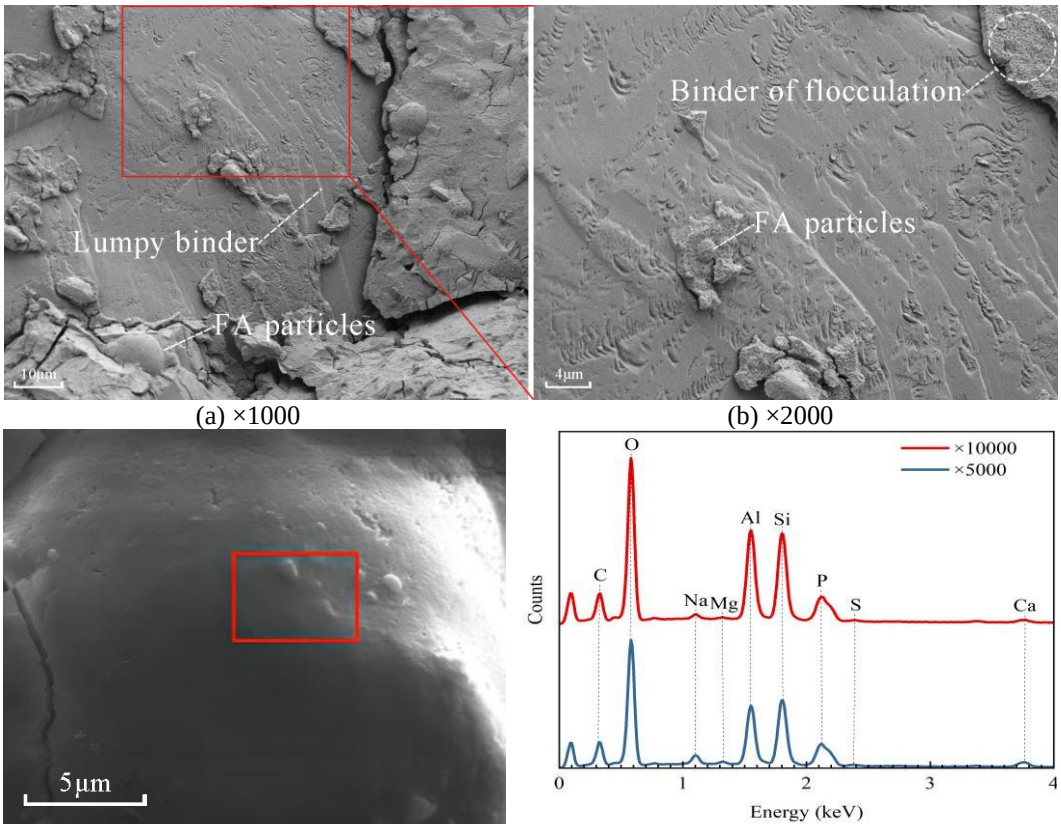

(a) ×1000 (b) ×2000

(c) EDS of F3G7C0 specimen after 28-day curing

Fig. 9. SEM-EDS results of F3G7C0 specimen after 28-day curing

As can be seen from **Fig. 9(a)**, when FA/GGBS = 3:7, the reaction degree of geopolymer mortars is relatively high, with no significant unreacted particles visible. Only a few large spherical FA particles wrapped in honeycomb-like gels are observed. These honeycomb-like gels are formed by the reaction of the amorphous phase inside FA after the FA is destroyed in the FA/GGBS matrix, generating tobermorite, which aggregates into crystals [30]. These gels are distributed around FA particles, indicating that the FA is eroded and damaged in an alkaline environment, allowing the internal mineral components to participate in the polymerization reaction. Additionally, as shown in **Fig. 9(b)**, the high degree of reaction generates lamellar gels that interconnect with each other, forming a highly compact overall structure. These gels also fill voids, resulting in a smooth surface structure with few microcracks, which tightly bonds with standard sand. These factors collectively enhance the mechanical properties of the mortar. On a macroscopic level, F3G7C0 exhibits the best mechanical performance.

As shown in the EDS spectrum in **Fig. 9(c)**, the reaction products of F3G7C0 are composed of elements such as C, O, Al, Si, P, Na, Mg, Ca, and S. The atomic ratios of Ca/Si, Al/Si, and Na/Si are 0.17, 0.79, and 0.13, respectively. Among the metal elements, Al and Na have the highest contents,

which is due to the high Al_2O_3 and Na_2O content in GGBS, FA, and the alkali activator. These components provide a rich supply of Al and Na elements for the formation of N-A-S-H and C-A-S-H gels, which will contribute to the improvement of the mechanical properties of the mortar.

For F5G5C0, as can be seen from **Figs. 10(a)** and **10(b)**, compared with **Figs. 9(a)** and **9(b)**, the gel structure in F5G5C0 exhibits a lower degree of compactness. Flocculent gels that are not tightly interconnected are dispersed within the structure, and a greater number of microcracks are present. This might be because as the content of GGBS decreases, the amount of calcium in the system is reduced, resulting in the formation of less C-A-S-H and C-S-H gels. These gels cannot form a cohesive network or effectively fill microcracks. Additionally, a significant number of FA spherical structures remain intact in the alkaline environment, preventing their participation in the polymerization reaction. This also contributes to the decline in mechanical properties.

From the EDS spectrum of F5G5C0 (**Fig. 10(c)**), it can be observed that the reaction products are similar to those of F3G7C0. However, the atomic ratios of Ca/Si, Al/Si, and Na/Si are 0.51, 0.34, and 0.31, respectively. The higher proportions of Ca, Al, and Na indicate that hydration reactions generated C-S-H (C-A-S-H) and N-A-S-H gels. However, the increase in atomic ratio does not mean that more gel products have been generated compared to F3G7C0.This is because the SiO_2 content in GGBS is as high as 52.95%, whereas the SiO_2 content in FA is only 30.22%. The reduction in GGBS content decreases the total amount of Si, limiting the formation of Si-based reaction products.

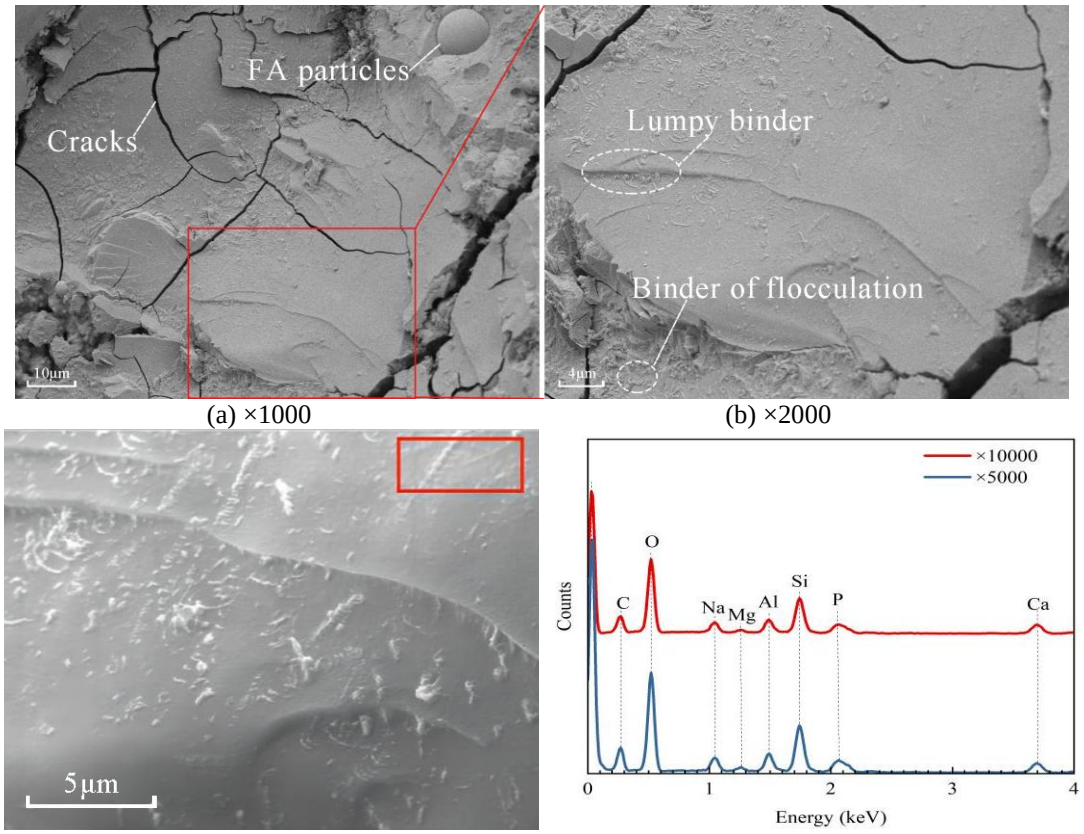

(a) ×1000 (b) ×2000

(c) EDS of F5G5C0 specimen after 28-day curing

Fig. 10. SEM-EDS results of F5G5C0 specimen after 28-day curing

Fig. 11 presents the microstructure and EDS spectrum of F7G3C0. From **Figs. 11(a)** and **11(b)**, it can be observed that, compared to F3G7C0 and F5G5C0, a larger amount of FA in this mixture remains unreacted. Although the generated gel appears to form an overall structure, it contains a significant number of unreacted FA particles. Additionally, SEM images reveal the presence of numerous cracks. These factors collectively result in the lowest 28-day mechanical strength among the three groups (F3G7C0, F5G5C0, and F7G3C0).

Fig. 11(c) shows the EDS spectrum of the F7G3C0 sample. It indicates a higher proportion of Si, Ca, Al, and Na elements. However, based on the sampling location, it can be inferred that this area

contains a considerable amount of quartz sand, which contributes to the elevated Si content.

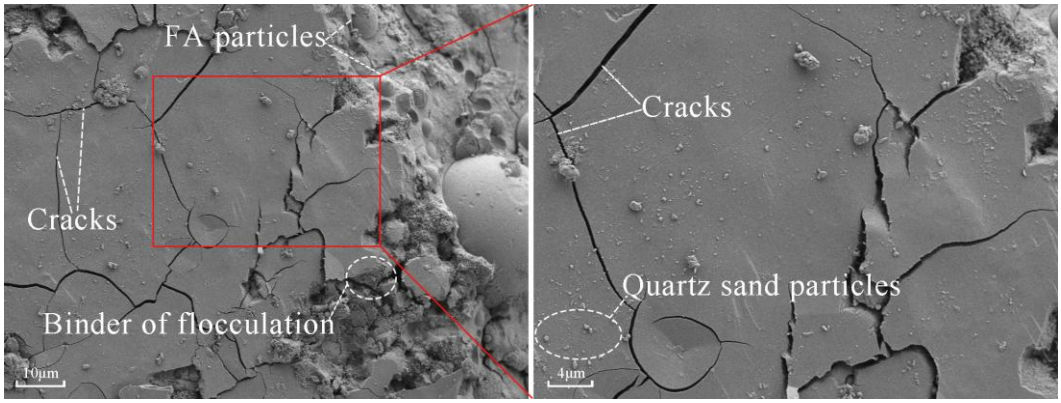

(a) ×1000 (b) ×2000

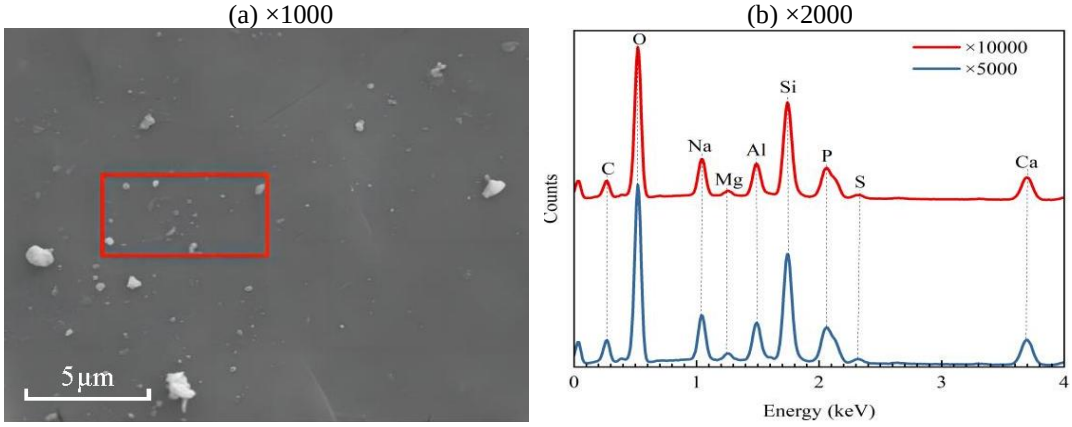

(c) EDS of F7G3C0 specimen after 28-day curing

Fig. 11. SEM-EDS results of F7G3C0 specimen after 28-day curing

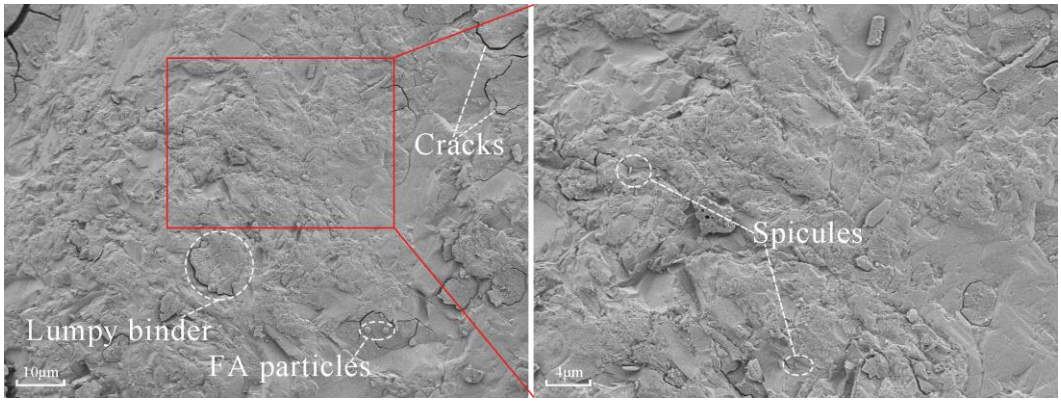

(a) ×1000 (b) ×2000

Fig. 12. SEM results of F5G5C0.1 specimen after 28-day curing

Fig. 12 shows the SEM images of F5G5C0.1. Compared with **Figs. 10(a)** and **10(b)**, the addition of CNC significantly reduces surface cracks in the sample. As shown in **Fig. 10(a)**, abundant cracks ranging from 0.5–2 μm are observed, while only sparse cracks exist in the F5G5C0.1. Moreover, the number of large FA particles is also reduced. Because CNC can attach to the surface of FA particles and form pathways into their interior, promoting the hydration reaction inside the FA and generating more hydration products. Additionally, due to the high aspect ratio of CNC, which resembles a rod-like shape [31], this feature is evident in **Fig. 12(b)**. CNC effectively bridges the gaps between cracks within the system, enhancing the material's strength. This phenomenon elucidates at the microstructural level through two distinct mechanisms why the F5G5C0.1 exhibits a 22.16% increase in flexural strength compared to F5G5C0.

4 Conclusions

This research comprehensively investigated the effects of FA/GGBS mass ratio (3:7, 5:5, and 7:3) and CNC dosage (0%, 0.10%, 0.20%, and 0.30% by the mass of mineral admixtures) on the performance of FA/GGBS-based geopolymer mortars. Some key conclusions are summarized:

Increasing the content of GGBS in the FA/GGBS based geopolymer mortar will result in a decrease in the fluidity of the system. For instance, When the ratio of FA/GGBS decreased from 7:3 to 3:7, the fluidity reduces by 17.56%. Although the increase in GGBS content reduces the fluidity of the FA/GGBS based geopolymer mortar, it can enhance its mechanical properties. This is because the CaO content in geopolymers is closely related to the rate of strength development and the achievable ultimate strength. Increasing the CaO content significantly accelerates the development rate of mechanical strength and enhances ultimate strength.

Adding CNC reduces the fluidity of FA/GGBS-based geopolymer mortars. For example, at an FA/GGBS ratio of 5:5, increasing the CNC content from 0% to 0.30% decreases fluidity by 33.47%. Although adding CNC to the system will reduce its fluidity, adding CNC to the system can enhance the long-term mechanical properties of FA/GGBS-based geopolymer mortar. Particularly, at an FA/GGBS ratio of 5:5, adding 0.10% CNC by the mass of mineral admixtures increases flexural and compressive strength by 22.16% and 2.74%, respectively.

Microstructural analysis using IC and SEM-EDS revealed that increasing GGBS content and adding CNC enhance the reaction activity and structural compactness of FA/GGBS-based geopolymer mortars. This improvement contributes to the enhancement of their mechanical performance.

Acknowledgements

The authors wish to acknowledge the China Postdoctoral Science Foundation (Grant No. 2023T160594) and the Key Research and Development Project of Henan Province (Grant No. 231111321000).

CRediT authorship contribution statement

Aofei Guo: Investigation, Conceptualization, Funding acquisition, Supervision, Writing – review & editing; **Haowei Ma:** Writing – original draft, Formal analysis; **Wenming Yang:** Investigation; **Hu Feng:** Funding acquisition, Writing – review & editing; **Liusheng Chu:** Supervision, Investigation, Writing – review & editing; **Zhihui Sun:** Writing – review & editing; **Zhenyun Yu:** Writing – review & editing.

Conflicts of Interest

The authors declare that they have no conflicts of interest to report regarding the present study.

Data Availability Statement

Some or all data, models, or codes that support the findings of this study are available from the corresponding author upon reasonable request.

References

[1] Peng JX, Huang L, Zhao YB, Chen P, Zeng L and Zheng W. Modeling of Carbon Dioxide Measurement on Cement Plants. Advanced Materials Research 2012; 610-613: 2120-2128. https://doi.org/10.4028/www.scientific.net/AMR.610-613.2120.

[2] Davidovits J, Geopolymer chemistry and applications, Geopolymer Institute, 2008.

[3] Shubbar AA, Sadique M, Kot P and Atherton W. Future of clay-based construction materials–A review. Construction and Building Materials 2019; 210: 172-187. https://doi.org/10.1016/j.conbuildmat.2019.03.206.

[4] Komljenović M, Baščarević Z and Bradić V. Mechanical and microstructural properties of alkali-activated fly ash geopolymers. Journal of Hazardous Materials 2010; 181(1-3): 35-42. https://doi.org/10.1016/j.jhazmat.2010.04.064.

[5] Meyer C. The greening of the concrete industry. Cement and Concrete Composites 2009; 31(8): 601-605. https://doi.org/10.1016/j.cemconcomp.2008.12.010.

[6] Domingues RM, Gomes ME and Reis RL. The potential of cellulose nanocrystals in tissue engineering strategies. Biomacromolecules 2014; 15(7): 2327-2346. https://doi.org/10.1021/bm500524s.

[7] Moon RJ, Martini A, Nairn J, Simonsen J and Youngblood J. Cellulose nanomaterials review: structure, properties and nanocomposites. Chemical Society Reviews 2011; 40(7): 3941-3994. https://doi.org/10.1039/C0CS00108B.
[8] Habibi Y, Lucia LA and Rojas OJ. Cellulose Nanocrystals: Chemistry, Self-Assembly, and Applications. Chemical Reviews 2010; 110(6): 3479-3500. https://doi.org/10.1021/cr900339w.
[9] Wang Y, Goodman S, Bao Y and Meng W. Morphological, microstructural, and mechanical properties of highly-ordered C–S–H regulated by cellulose nanocrystals (CNCs). Cement and Concrete Composites 2023; 143: 105276. https://doi.org/10.1016/j.cemconcomp.2023.105276.
[10] Zheng D, Yang H, Feng W, Fang Y and Cui H. Modification mechanism of cellulose nanocrystals in cement. Cement and Concrete Research 2023; 165: 107089. https://doi.org/10.1016/j.cemconres.2023.107089.
[11] Cao Y, Zavaterri P, Youngblood J, Moon R and Weiss J. The influence of cellulose nanocrystal additions on the performance of cement paste. Cement and Concrete Composites 2015; 56: 73-83. https://doi.org/10.1016/j.cemconcomp.2014.11.008.
[12] Grishkewich N, Mohammed N, Tang J and Tam KC. Recent advances in the application of cellulose nanocrystals. Current Opinion in Colloid & Interface Science 2017; 29: 32-45. https://doi.org/10.1016/j.cocis.2017.01.005.
[13] Lee H-J, Kim S-K, Lee H-S and Kim W. A study on the drying shrinkage and mechanical properties of fiber reinforced cement composites using cellulose nanocrystals. International Journal of Concrete Structures and Materials 2019; 13: 1-11. https://doi.org/10.1186/s40069-019-0351-2.
[14] Rahmawati C, Aprilia S, Saidi T, Aulia TB, Amin A, Ahmad J and Isleem HF. Mechanical properties and fracture parameters of geopolymers based on cellulose nanocrystals from Typha sp. fibers. Case Studies in Construction Materials 2022; 17: e01498. https://doi.org/10.1016/j.cscm.2022.e01498.
[15] Feng H, Bilal I, Sun Z, Guo A, Yu Z, Du Y, Su Y and Zheng Y. Mechanical and shrinkage properties of cellulose nanocrystal modified alkali-activated fly ash/slag pastes. Cement and Concrete Composites 2024; 154: 105753. https://doi.org/10.1016/j.cemconcomp.2024.105753.
[16] Luukkonen T, Abdollahnejad Z, Yliniemi J, Kinnunen P and Illikainen M. One-part alkali-activated materials: A review. Cement and Concrete Research 2018; 103: 21-34. https://doi.org/10.1016/j.cemconres.2017.10.001.
[17] Duxson P and Provis JL. Designing precursors for geopolymer cements. Journal of the American Ceramic Society 2008; 91(12): 3864-3869. https://doi.org/10.1111/j.1551-2916.2008.02787.x.
[18] Roopchund R, Andrew J and Sithole B. Using cellulose nanocrystals to improve the mechanical properties of fly ash-based geopolymer construction materials. Engineering Science and Technology, an International Journal 2022; 25: 100989. https://doi.org/10.1016/j.jestch.2021.04.008.
[19] Li Z, Chen Y, Provis JL, Cizer Ö and Ye G. Autogenous shrinkage of alkali-activated slag: A critical review. Cement and Concrete Research 2023; 172: 107244. https://doi.org/10.1016/j.cemconres.2023.107244.
[20] 1346-2011 CNSGT, Test methods for water requirement of normal consistency, setting time and soundness of the portland cement (in Chinese).
[21] 17671-2021 CNSGT, Test method of cement mortar strength (ISO method)(In Chinese).
[22] Khan MZN, Hao Y and Hao H. Synthesis of high strength ambient cured geopolymer composite by using low calcium fly ash. Construction and Building Materials 2016; 125: 809-820. https://doi.org/10.1016/j.conbuildmat.2016.08.097.
[23] Feng H, Xin X, Guo A, Yu Z, Shao Q, Sheikh MN and Sun Z. Effect of mix proportion parameters on chloride erosion resistance of fly ash/slag-based engineered geopolymer composites. Journal of Cleaner Production 2024; 438: 140785. https://doi.org/10.1016/j.jclepro.2024.140785.
[24] Somna R, Jaturapitakkul C, Chalee W and Rattanachu P. Effect of the water to binder ratio and ground fly ash on properties of recycled aggregate concrete. Journal of Materials in Civil Engineering 2012; 24(1): 16-22. https://doi.org/10.1061/(ASCE)MT.1943-5533.0000360.
[25] Yang T, Yao X and Zhang Z. Quantification of chloride diffusion in fly ash–slag-based geopolymers by X-ray fluorescence (XRF). Construction and Building Materials 2014; 69: 109-115. https://doi.org/10.1016/j.conbuildmat.2014.07.031.
[26] Song W, Zhu Z, Peng Y, Wan Y, Xu X, Pu S, Song S and Wei Y. Effect of steel slag on fresh, hardened and microstructural properties of high-calcium fly ash based geopolymers at standard curing condition. Construction and Building Materials 2019; 229: 116933. https://doi.org/10.1016/j.conbuildmat.2019.116933.
[27] Eduok E, Thermal properties of geopolymer materials, University of Stavanger, Norway, 2016.
[28] Mohamed R, Abd Razak R and Al Bakri Abdullah MM. A Review on Heat Released in early Geopolymerization by Calorimetric Study. Materials Science Forum 2019; 967: 236-240. https://doi.org/10.4028/www.scientific.net/MSF.967.236.
[29] Kumar S, Kumar R and Mehrotra S. Influence of granulated blast furnace slag on the reaction, structure and properties of fly ash based geopolymer. Journal of Materials Science 2010; 45(3): 607-615. https://doi.org/10.1007/s10853-009-3934-5.

[30] Da Y, Laixue P, Di S, Mingyang L, Jiabin W and Zebin G. Reaction Mechanism of Fly Ash in Alkali-Activated Slag/Fly Ash System. Bulletin of the Chinese Ceramic Society 2021; 40(9): 3005. https://research.ebsco.com/linkprocessor/plink?id=24f2daa9-92e6-3f5a-8083-67ef014b14c4.

[31] Appidi T, Sushma MV and Rengan AK, Cellulose Nanocrystals, in: A. Barhoum (Ed.) Handbook of Nanocelluloses: Classification, Properties, Fabrication, and Emerging Applications, Springer International Publishing, Cham, 2020; 1-31.